Predicted Behaviour of Saturated Granular Waste Blended with Rubber Crumbs

Yujie Qi
PhD, MSc, BSc
Research Associate, Centre for Geomechanics and Railway Engineering, ARC Industry Transformation Training Centre for Advanced Rail Track Technologies, Faculty of Engineering & Information Science, University of Wollongong, Wollongong, NSW 2522, Australia

Buddhima Indraratna
PhD (Alberta), MSc and BSc-Hons (London), FTSE, FIEAust, FASCE, FGS, FAusIMM, FIES, DIC, CEng, CPEng
Distinguished Professor, Research Director and Foundation Director, Civil Engineering, Centre for Geomechanics and Railway Engineering, ARC Industry Transformation Training Centre for Advanced Rail Track Technologies, Faculty of Engineering & Information Science, University of Wollongong, Wollongong, NSW 2522, Australia

Matthew Richard Coop
PhD
Professor, Department of Civil, Environmental & Geomatic Engineering, Faculty of Engineering Science, University College London, U.K.

†Author for correspondence:
Distinguished Prof. Buddhima Indraratna
School of Civil, Mining & Environmental Engineering,
Faculty of Engineering and Information Science,
University of Wollongong Australia
Wollongong, NSW 2522
AUSTRALIA
Ph: +61 2 4221 3046
Fax: +61 2 4221 3238
Email: indra@uow.edu.au

To be submitted to: International Journal of Geomechanics

Abstract: Recycling waste materials such as steel furnace slag (SFS), coal wash (CW), and rubber crumbs (RC) for transport infrastructure is environmentally friendly and offers significant economic benefits. This paper presents a fundamental study of the geotechnical characteristics of this blended matrix (SFS+CW+RC). A semi-empirical constitutive model for SFS+CW+RC mixtures is proposed within the framework of critical state soil mechanics and based on the bounding surface plasticity theory. A critical state surface is formulated with the changing RC contents in the waste mixtures, and an experimental relationship between the total work input (W_{total}) and critical state parameter (M_{cs}) is established to capture the energy absorbing capacity of the matrix. The theoretical model is validated using two sets of data, i.e. very recent triaxial test data obtained by the authors and totally independent test results from a past study conducted on sand-RC mixtures.

KEYWORDS: Steel furnace slag; coal wash; rubber crumbs; critical state; energy absorbing property; constitutive model; bounding surface plasticity

Introduction

Steel furnace slag (SFS) and coal wash (CW) are granular waste by-products of the steel manufacturing and coal mining industry, respectively. Rubber crumbs (RC) are derived from waste tires. However, these waste granular materials cannot be used individually because of their adverse geotechnical properties, i.e. the expansive potential of SFS, the particle degradation of CW and the high deformation of rubber materials (Indraratna et al. 1994; Heitor et al. 2016; Wang et al. 2010; Lee et al. 1999). To minimize the detrimental effect of these waste materials, they are usually mixed with other materials prior to their adoption in civil engineering. SFS is usually blended with fly ash, cement, dredged materials, asphalt, or concrete to be used in landfill or pavements (Xue et al. 2006; Yildirim and Prezzi 2015; Lizarazo-Marriaga et al. 2011; Malasavage et al. 2012). RC usually mixed with sand, clay, fine-grained soil, fine recycled glass, crushed rock or asphalt to serve as lightweight landfill, highway embankments, flexible or permeable pavements, as well as for applications in seismic isolation (Fu et al. 2017; Ajmera et al. 2017; Lee et al. 1999; Li et al. 2016; Tsang et al. 2012; Sheikh et al. 2013; Disfani et al. 2017; Mohammadinia et al. 2018; Yaghoubi et al. 2018). It is reported that the blends of SFS and CW can reduce the swelling of SFS and the particle breakage of CW, and a SFS+CW mixture with an appropriate ratio of SFS:CW has been successfully applied in Wollongong port reclamation (Chiaro et al. 2013; Tasalloti et al. 2015). To extend the application of SFS+CW mixtures into dynamic loading projects (e.g. railway subballast), RC was considered favourably in the granular matrix to enhance the energy absorbing property as described by Indraratna et al. (2018).

The geotechnical properties of SFS+CW+RC mixtures under static loading have already been investigated earlier by Indraratna et al. (2018), Qi et al. (2018a), and Qi et al. (2018b). The test results indicate that incorporating RC into SFS+CW blends can further reduce particle breakage in CW and swelling of SFS. However, a more insightful understanding of the effect that RC has on the geotechnical behaviour of these waste granular mixtures can be attained from a mathematical perspective capturing the enhanced energy absorbing capacity of RC blends. Despite previous laboratory research carried out to investigate the behaviour of soil-rubber mixtures, only a few have focused on the theoretical models within a constitutive framework.

Lee et al. (1999) proposed a hyperbolic model to predict the static stress-strain behaviour of sand-tire mixtures, but it could not capture the post-peak phenomenon of the deviator stress-strain curves. Other previous studies such as Youwai and Bergado (2003) and Mashiri et al. (2015a) modelled the static behaviour of sand-shred tire/tire chips mixtures using a hypoplasticity model, but none of them considered the energy absorbing capacity of rubber materials. Youwai and Bergado (2003) indicated that for $30\% < RC\ contents\ (R_b) < 100\%$, sand-RC blends could barely achieve a critical state (CS) under laboratory conditions, so the condition at the end of the test could only be postulated to reach CS, which is the same approach adopted by Disfani et al. (2017) for recycled glass-tire mixtures; this is partly the reason why the model predictions and experimental data have diverged. Therefore, obtaining more realistic CS parameters is the key requirement to develop a constitutive model within the framework of critical state for soil-RC mixtures.

Mashiri et al. (2015b) found that mixtures of sand-tire chips could not attain CS, and Fu et al. (2014) also experienced difficulty in achieving a distinct CS for sand-tire fibre mixtures even at larger axial strains. However, Qi et al. (2018a) indicates that SFS+CW+RC mixtures with low RC contents (<20%) can achieve a CS, and for those with higher RC contents there is still a possibility of attaining a CS at larger axial strain. This could be attributed to the fact that the different shapes of various rubber additives were expected to have different packing (compaction) arrangements upon loading; for instance, granulated rubber may impose a stress-strain and volumetric behaviour different to that of tire chips or fibres (Fu et al. 2017; Mashiri et al. 2017). Further, the obvious differences in grain shapes and hardness as well as totally different chemical compositions of SFS and CW compared to say natural sand (quartz) will induce distinct differences in particle densification upon loading, variations in inter-particulate friction and grain degradation, apart from other physical and geotechnical characteristics. CW particles are usually a random blend of both angular and relatively flaky grains and are of dual porosity (Indraratna et al. 2018; Heitor et al. 2016), while SFS aggregates compose mainly of prismoidal/cuboidal particles with strong interlocking properties thus reducing potential shear failure, but undergo noticeable swelling in the presence of moisture (Shi 2004). More recently, Heitor et al. (2016) demonstrated that for compacted CW, the critical state line (CSL) shifts downwards significantly with respect to the $e - \ln p'$ plane (i.e. void ratio vs mean effective stress) due to particle degradation. Chiaro et al. (2015) found that the CSL for SFS+CW blends was not unique and was sensitive to the mix proportions and the extent of grain degradation upon loading. In view of the abovementioned reasons, experimental observations from past studies conducted on soil-rubber chips/fibre mixtures or traditional granular soils such as sands cannot be extrapolated to interpret or predict the behaviour of the current SFS+CW+RC matrix.

Qi et al. (2018a) recently reported that R_b (%) has a significant influence on the critical state and the dilatancy behaviour of SFS+CW+RC mixtures, i.e. as R_b (%) increases, the dilatancy and the slope of the critical state line in $e - \ln p'$ space decreases. Moreover, Qi et al. (2018a) also introduced an empirical function between the total work input and the critical state stress ratio to capture the energy absorbing property of the waste mixtures in a dilatancy model, and with this empirical model the critical state parameters of the waste mixtures can be obtained more precisely. In this context, a constitutive model for SFS+CW+RC mixtures under static loading condition extending the bounding surface plasticity theory (Dafalias and Popov 1975) within the framework of critical state is proposed in this paper, and this model is able to simulate strain softening and stress dilatancy for materials compacted in a dense condition more accurately.

To support the fundamental constitutive behaviour, the experimental results of a series of consolidated drained triaxial tests conducted on initially fully saturated SFS+CW+RC mixtures (with SFS:CW=7:3, $R_b = 0, 10, 20, 30, \text{and } 40\%$) by Qi et al. (2018a) have been adopted. The degree of saturation close to unity was established using the Skempton's B value ≥0.98. Membrane correction was applied for the test results obtained under $\sigma'_3 = 10\ kPa$, while for higher effective confining pressures the membrane effect was ignored as the error was less than 3% (Indraratna et al. 2018; Lackenby et al. 2007). In Australia, there are many low-lying coastal tracks in which the subballast is usually saturated by the high groundwater table (Qi et al. 2018c). To predict the stress-strain behaviour more accurately, the influence of R_b (%) on the critical state of SFS+CW+RC specimens compacted at 95% of their maximum dry density and sheared under three different effective confining pressures ($\sigma'_3 = 10, 40, \text{and } 70\ kPa$) have been studied. The proposed model is then verified by the experimental data obtained by the authors for SFS+CW+RC mixtures as well as totally independent data obtained from a past study for sand-RC mixtures (Youwai and Bergado 2003).

The critical state of the granular waste mixtures

Fig.1 shows the typical stress paths of monotonic triaxial tests in $q - p'$ plane and the stress ratio-dilatancy curves for SFS+CW+RC with $R_b = 10\%$ and 40%. In Fig.1 (a-b), the phase transformation state (PTS) line and the critical state line (CSL) are given, and the stress ratio according to these two special states is defined by (Fig.1 a-b):

$$\eta_{PTS,CS} = \frac{q_{PTS,CS}}{p'_{PTS,CS}} \tag{1}$$

where $q = \sigma'_1 - \sigma'_3$ is the deviator stress, $p = (\sigma'_1 + 2\sigma'_3)/3$ is the effective mean stress, and the critical stress ratio η_{CS} can also be written as M_{cs}.

At the phase transformation state, as the volumetric strain ε_v reaches a minimum value, the specimen changes from contraction to dilatancy, i.e. the dilatancy $d = d\varepsilon_v^p / d\varepsilon_q^p = 0$ (Fig.1 c-d), where $d\varepsilon_v^p$ and $d\varepsilon_q^p$ are the incremental plastic volumetric strain and incremental plastic deviator strain, respectively. At the critical state, the specimen reaches a constant stress condition upon further straining at which the dilatancy d also reaches zero. Note that the dilatancy of the waste granular mixtures decreases as σ'_3 and R_b increase (Fig.1 c-d). It was reported that under laboratory conditions, only the SFS+CW+RC mixtures with $R_b < 20\%$ could reach a critical state, whereas those with higher R_b (20-40%) indicated the potential for attaining a critical state beyond the ultimate strain condition as evaluated in the laboratory (Qi et al. 2018a). This may be attributed to the addition of RC that changes the skeleton of the granular matrix. When $R_b \geq 20\%$, the skeleton of the specimen is overly influenced by RC (Qi et al. 2018c). Therefore, the critical state of the granular mixtures ($R_b \geq 20\%$) could be determined by extrapolation (Qi et al. 2018a), following the technique first introduced by Carrera et al. (2011).

The waste mixtures which were prepared at a relatively dense state represented a phase transformation stress ratio η_{PTS} greater than the critical stress ratio M_{cs} (Fig.1 a-b). As R_b increases from 10% to 40%, the slopes of the phase transformation line and the CSL decrease. Moreover, the CSL exhibits an apparent cohesion interception when $p' = 0$. This is in line with previous studies of sand-rubber mixtures tested by Mashiri et al. (2015b), Zornberg et al. (2004), and Youwai and Bergado (2003), which means that the critical stress ratio is no longer a constant for each SFS+CW+RC mixture, and it changes with R_b and σ'_3.

Generally it is assumed that the critical state ratio (M_{cs}) or the friction angle at critical state is constant and independent of density, but for most granular materials M_{cs} may vary depending on the shearing mechanisms at a particular level as well as materials fabric and initial anisotropy (Been et al. 1991), albeit limited evidence available from past literature. Changes in the critical state ratio M_{cs} can occur in materials such as ballast and rockfill that are subjected to substantial particle breakage, as reported by Indraratna et al. (2015) and Chavez and Alonso (2003). Although it has been reported that the particle breakage would not affect the consistency of M_{cs} for natural sand (Coop 1990; Coop et al. 2004), the shearing behaviour and particle breakage can be significantly different in other types of granular assemblies including rail ballast or coarse rockfill due to their considerably varied particle sizes and shapes (angularity) when compared to relatively finer sands and gravels as often used in traditional small-scale geotechnical testing. Variation in M_{cs} can also occur to the granular mixtures when RC is included such as SFS+CW+RC mixtures examined by Indraratna et al. (2018), and Qi et al. (2018a), and sand-RC mixtures tested by Youwai and Bergado (2003), Mashiri et al. (2015b), and Fu et al. (2014; 2017). The inclusion of RC reduces particle breakage as also reported by Fu et al. (2014), probably because of the increased energy absorbing capacity of the matrix, while providing a 'cushioning' effect to the otherwise more brittle grains. Indraratna et al. (2018) examined the strain energy density of SFS+CW+RC mixtures and found that 10% inclusion of RC could cause a 2-3 fold increase in the strain energy density. Further, for all the RC-soil mixtures, the addition of RC could transform the stress-strain curve from a brittle to a relatively ductile behaviour with strain hardening (Indraratna et al. 2018; Qi et al. 2018a; Zornberg et al. 2004; Mashiri et al. 2015a). It can be assumed that part of work input causing particle breakage is now absorbed through greater deformation attributed to the addition of RC, which is also in agreement with Fu et al (2014). It seems that the work input is a good indicator of conditions leading to particle breakage and deformation. To reflect more on the variable critical state parameter M_{cs} induced by particle breakage, Chavez and Alonso (2003) introduced the plastic work. Moreover, to represent the influence of the enhanced energy absorbing capacity (due to the increasing R_b) on M_{cs}, the total work input up to failure (W_{total}) was introduced earlier by Qi et al. (2018a) (Equations 2-3; Fig.2a). Note that failure here is defined when the specimen achieves its peak deviator stress in the same way as explained by Zornberg et al. (2004) for sand-RC mixtures. In view of the above:

$$dW_{total} = p'd\varepsilon_v + qd\varepsilon_q \tag{2}$$

$$M^*_{cs}(W_{total}) = M_0 * (\frac{W_{total}}{W_0})^\alpha \tag{3}$$

where M_0 is the critical stress ratio when $W_{total} = 1\ kPa$, α is a regression coefficient, and $W_0 = 1\ kPa$ corresponds to M_0. The work is expressed in units of work per unit volume of specimen, so the unit of work here considered to be the same as stress (i.e. kN/m^2 or kPa).

It is interesting to note that this empirical relationship between W_{total} and M_{cs} also applies to other RC-soil mixtures such as sand-RC mixtures (Youwai and Bergado 2003; Fig.2b), and it can also be extended to other materials which have varying value of M_{cs}, such as ballast (Indraratna et al. 2015; Fig.2c) and rockfill, albeit the omission of elastic work input by Chavez and Alonso (2003) (Fig.2d). This indicates that W_{total} is a unique parameter that relates to M_{cs} for materials having variable critical stress ratios. Therefore, this can provide a convenient way to obtain the critical state parameters for those materials with changing M_{cs} that cannot reach a critical state using laboratory tests.

Based on Equations (1-3), a critical state surface can be generated for SFS+CW+RC mixtures in the in $q_{cs} - p_{cs} - W_{total}$ space (Fig.3). Although the plotted points scatter on the work input surface, a large difference in W_{total} between the waste mixtures with 0% and $\geq$ 10% RC under the same σ'_3 can be observed, indicating a significant increase in energy absorbing capacity with the addition of RC, and this difference increases as σ'_3 increases.

For each SFS+CW+RC mixture, the CSL in $e - \ln p'$ space presents a linear relationship (Fig.4):

$$e_{cs} = \Gamma^* - \lambda^* \ln p'_{cs} \quad (4)$$

where Γ^* is the void ratio at $p'_{cs} = 1\ kPa$, and λ^* is the gradient of the critical state line in $e - \ln p'$ space. Note that the CSL for these waste mixtures is not unique, and it rotates clockwise as R_b (%) increases (Fig.4). Qi et al. (2018a) found earlier that Γ^* and λ^* are in a linear relationship with R_b:

$$\Gamma^*(R_b) = \Gamma_1 + \Gamma_2 R_b \quad (5)$$

$$\lambda^*(R_b) = \lambda_1 + \lambda_2 R_b \quad (6)$$

where $\Gamma^*(R_b)$ and $\lambda^*(R_b)$ are the critical state parameters as influenced by R_b. The parameters Γ_1, Γ_2, λ_1 and λ_2 are the regression indices calculated by laboratory test data of the granular waste matrix with SFS:CW=7:3 and $R_b = 0 - 40\%$ (Fig.4). This established relationship for SFS+CW+RC mixtures also suits sand-RC mixtures (data taken from Youwai and Bergado 2003). The values for the critical state parameters for SFS+CW+RC mixtures and sand-RC mixtures are shown in Table 1.

Substituting Equations (5) and (6) into Equation (4), produces the critical state surface shown in Fig.5, which can be described using Equation (7) as follows:

$$e_{cs} = (\Gamma_1 + \Gamma_2 R_b) - (\lambda_1 + \lambda_2 R_b) \ln p'_{cs} \quad (7)$$

Bounding surface and loading surface

In this study, the concept of bounding surface first introduced by Dafalias and Popov (1975) is applied due to its versatility and its ability to accurately reproduce the stress-strain behaviour of various soil types (Russell and Khalili 2006; Sun et al. 2014).

The bounding surface is shaped as a half tear drop that encompasses the triaxial compression part. To facilitate further analysis, the loading surface is assumed to follow the same shape as the bounding surface, i.e. the bounding surface $F(\bar{p}', \bar{q}, \bar{p}'_c) = 0$ and the loading surface $f(p', q, p'_C) = 0$ for the SFS+CW+RC mixtures inspired by Russell and Khalili (2006):

$$F(\bar{p}', \bar{q}, \bar{p}'_c) = \left\{\bar{q} + M_{cs}^*(W_{total})(\bar{p}')\left[N \ln(\frac{\bar{p'}}{\bar{p'}_C})\right]^{1/N}\right\} = 0, \quad (8)$$

$$f(p', q, p'_C) = \left\{q + M_{cs}^*(W_{total})(p')\left[N \ln(\frac{p'}{p'_C})\right]^{1/N}\right\} = 0, \quad (9)$$

where $\bar{p}'_c$ and p'_C are the intercepts of the bounding surface and loading surface with $q = 0$ axis, respectively, controlling the size of the bounding surface and the loading surface (Fig.6). $M_{cs}^*(W_{total})$ is the critical stress ratio modified according to the total work input W_{total}. Thus W_{total} is an important parameter that indirectly influences the shape of the bounding surface and the loading surface, as reflected by Equations (8-9). $N \geq 1$ is a material constant that controls the curvature of the bounding surface. A material constant R is used here to express the ratio between p' at the intercept of the loading surface with M_{cs} line and the image point p'_C; and the ratio between $\overline{p'}$ at the intercept of the loading surface with M_{cs} line and the image point $\overline{p'}_C$ (Fig.6), hence:

$$R = \frac{p'}{p'_C} = \frac{\overline{p'}}{\overline{p'}_C} \quad (10)$$

By using a radial mapping rule, the stress ratio can be written as:

$$\eta = \frac{q}{p'} = \frac{\bar{q}}{\overline{p'}}. \quad (11)$$

By combining Equations (8-11), the ratio R can then be calculated from:

$$R = exp\left[-\frac{1}{N}(\frac{\eta}{M_{cs}^*(W_{total})})^N\right]. \quad (12)$$

Note that M_{cs} decreases exponentially with the total work input W_{total} (Fig.2a), indicating decreased R with W_{total}. The evolution of the bounding surface is controlled by $\bar{p}'_c$ which is related to the evolution of the volumetric strain, and the corresponding swelling line represented by:

$$e = e_{\kappa 0} - \kappa \ln p' \tag{13}$$

By recalling Equations (4-6, 10), the position of $\bar{p}'_c$ on the bounding surface can be determined by:

$$\bar{p}'_c = \frac{p'_r}{R} exp\left(\frac{\Gamma^*(R_b) - \mathrm{e} - \kappa \ln p'}{\lambda^*(R_b) - \kappa}\right) \tag{14}$$

where $e_{\kappa 0}$ is the void ratio when $p' = 1$ in Equation (13); p'_r is the unit pressure; κ is the gradient of the swelling line. Through $\Gamma^*(R_b)$ and $\lambda^*(R_b)$ the influence of R_b on $\bar{p}'_c$ as well as on the bounding surface and the loading surface can be incorporated.

The unit normal loading vector $\boldsymbol{n}$ at the image point on the bounding surface can then be calculated using the following (see derivations in Appendix 1):

$$\boldsymbol{n} = \frac{\partial F/\partial \bar{\boldsymbol{\sigma}}'}{\|\partial F/\partial \bar{\boldsymbol{\sigma}}'\|} = \left[\boldsymbol{n_p}, \boldsymbol{n_q}\right]^T =$$

$$\left[\frac{M^*_{cs}(W_{total})\left[N \ln\frac{\bar{p}'}{\bar{p}'_c}\right]^{\frac{1}{N}}\left[1+\left(N \ln\frac{\bar{p}'}{\bar{p}'_c}\right)^{-1}\right]}{\sqrt{\left\{M^*_{cs}(W_{total})\left[N \ln\frac{\bar{p}'}{\bar{p}'_c}\right]^{\frac{1}{N}}\left[1+\left(N \ln\frac{\bar{p}'}{\bar{p}'_c}\right)^{-1}\right]\right\}^2+1}}, \frac{1}{\sqrt{\left\{M^*_{cs}(W_{total})\left[N \ln\frac{\bar{p}'}{\bar{p}'_c}\right]^{\frac{1}{N}}\left[1+\left(N \ln\frac{\bar{p}'}{\bar{p}'_c}\right)^{-1}\right]\right\}^2+1}}\right]^T .$$

(15)

Where $\bar{\boldsymbol{\sigma}}'$ is the effective stress on the bounding surface; $\boldsymbol{n_p}$ and $\boldsymbol{n_q}$ are components of the loading direction vectors.

Plastic potential

The dilatancy of the material which is related to the plastic potential, represents the ratio between the incremental plastic volumetric strain and the plastic shear strain. Been and Jefferies (1985) reinvented a state parameter ψ inspired after Worth and Bassett (1965) to capture the influence that unit weight and applied stress have on the deformation of soil, where ψ is defined as the difference between the current void ratio and the critical void ratio at the same stress:

$$\psi = e - e_{cs} \tag{16}$$

As mentioned previously, the critical void ratio of the waste mixtures is related to R_b (%), therefore the state parameter ψ can be modified as:

$$\psi^*(R_b) = e - (\Gamma^*(R_b) - \lambda^*(R_b) \ln p'_{CS}) \tag{17}$$

Following Li and Dafalias (2000), the dilatancy (d) of soil is associated with the state parameter (ψ), and is expressed by:

$$d = \frac{d\varepsilon_v^p}{d\varepsilon_q^p} = \frac{\partial g/\partial p'}{\partial g/\partial q} = d_0 \left(e^{m\psi^*(R_b)} - \frac{\eta}{M_{cs}^*(W_{total})} \right) \tag{18}$$

Where g is the plastic potential; d_0 and m are two material parameters, $M_{cs}^*(W_{total})$ is the critical stress ratio modified in relation to W_{total}, and $\psi^*(R_b)$ is the state parameter modified with R_b (%).

With the dilatancy form of Equation (18), the plastic potential $g = 0$ can be attained by integration, and then the unit vector of plastic flow ($\boldsymbol{m}$) at $\boldsymbol{\sigma}'$ (the effective stress on the loading surface) can be generally defined by:

$$\boldsymbol{m} = \frac{\frac{\partial g}{\partial \boldsymbol{\sigma}'}}{\left\| \frac{\partial g}{\partial \boldsymbol{\sigma}'} \right\|} = \left[\boldsymbol{m_p}, \boldsymbol{m_q}\right]^T = \left[\frac{d}{\sqrt{1+d^2}}, \frac{1}{\sqrt{1+d^2}}\right]^T \quad (19)$$

where, $\boldsymbol{m}$ is the plastic flow direction vector; $\boldsymbol{m_p}$ and $\boldsymbol{m_q}$ are components of the plastic flow direction vectors.

Hardening rule

In light of the bounding surface concept, the hardening modulus $\boldsymbol{H}$ is divided into two components:

$$\boldsymbol{H} = \boldsymbol{H_b} + \boldsymbol{H_\delta} \quad (20)$$

where $\boldsymbol{H_b}$ is the plastic modulus at $\bar{\boldsymbol{\sigma}}'$ on the bounding surface and $\boldsymbol{H_\delta}$ is the arbitrary modulus at $\boldsymbol{\sigma}'$. $\boldsymbol{H_b}$ can be defined by adopting an isotropic hardening rule with changes in the plastic volumetric strain as follows (see derivations in Appendix 2):

$$\boldsymbol{H_b} = -\frac{\partial F}{\partial \bar{p}'_c}\frac{\partial \bar{p}'_c}{\partial \varepsilon_v{}^p}\frac{\boldsymbol{m_p}}{\|\partial F/\bar{\boldsymbol{\sigma}}'\|} \quad (21)$$

$$= \frac{M_{cs}^*(W_{total})p'\left[N\ln(\frac{\bar{p}'}{\bar{p}'_c})\right]^{\frac{1}{N}}}{\bar{p}'_c N\ln(\frac{\bar{p}'}{\bar{p}'_c})}\frac{1+e}{\lambda^*(R_b)-\kappa}\frac{d_0\left(e^{m\psi^*(R_b)}-\frac{\eta}{M_{cs}^*(W_{total})}\right)}{\sqrt{1+\left[d_0\left(e^{m\psi^*(R_b)}-\frac{\eta}{M_{cs}^*(W_{total})}\right)\right]^2}}\frac{1}{\sqrt{\left\{M_{cs}^*(W_{total})\left[N\ln\frac{\bar{p}'}{\bar{p}'_c}\right]^{\frac{1}{N}}\left[1+\left(N\ln\frac{\bar{p}'}{\bar{p}'_c}\right)^{-1}\right]\right\}^2+1}}$$

According to the bounding surface concept, $\boldsymbol{H_\delta}$ is a decreasing function of the distance between $\boldsymbol{\sigma}'$ and $\bar{\boldsymbol{\sigma}}'$ on the bounding surface (Khalili et al. 2008), and it can be taken as an arbitrary form:

$$\boldsymbol{H_\delta} = h_0\frac{\delta}{\delta_{max}-\delta}\frac{1+e}{\lambda^*(R_b)-\kappa}\frac{p'}{\bar{p}'_c}, \quad (22)$$

where h_0 is a scaling parameter controlling the steepness of the response in the $\varepsilon_v - \varepsilon_q$ plane. δ_{max} and δ are the distance from the stress origin and the current stress point to the image stress point, respectively (Fig.6). Due to the radial mapping rule, $\delta/(\delta_{max} - \delta)$ equals to $(\bar{p}'_c - p'_C)/p'_C$ (Fig.6). As $(1 + e)/[\lambda^*(R_b) - \kappa]$ stays positive, $\boldsymbol{H_\delta}$ is always positive, and only when $\bar{p}'_c = p'_C$, $\boldsymbol{H_\delta}$ reaches zero, at which $\boldsymbol{H} = \boldsymbol{H_b}$. When $\delta_{max} \leq \delta$, $\boldsymbol{H_\delta} = +\infty$, $\boldsymbol{H}$ becomes very large, and the response is purely elastic. When the magnitudes of $\boldsymbol{H_b}$ and $\boldsymbol{H_\delta}$ are equal but have the opposite sign, $\boldsymbol{H} = \boldsymbol{0}$, and at this point strain hardening transforms to strain softening.

Evaluation of model parameters

The parameters in this proposed model are divided into five categories: elastic, critical state, bounding surface, plastic potential, and the hardening domain. The parameters for the elastic part are explained in Appendix 3. All the parameters for SFS+CW+RC mixtures and sand-RC mixtures (data sourced from Youwai and Bergado 2003) are listed in Table 1 and Table 2, respectively.

The parameters α, M_0, Γ_1, Γ_2, λ_1 and λ_2 are related to establish the critical state surface, where α and M_0 can be obtained by fitting the relationship between work input and critical state stress ratio as shown earlier in Fig.2. The values of Γ_1, Γ_2, λ_1 and λ_2 can be determined via curve fitting as shown in Fig.4.

Parameter N defines the curvature of the bounding surface. It can be obtained by fitting $q{\sim}p'$ plot of the undrained triaxial tests on the loosest samples. Previous studies found $1 \leq N \leq 3$ for granular materials (Khalili et al. 2008; Russell and Khalili 2006; Russell and Khalili 2004; Sun et al. 2014). As no undrained tests for the waste mixtures were available herein, and the value of N was found to be insensitive in relation to the predicted results in this study, so $N = 1$ was assumed for simplicity.

d_0 and m are two parameters used in soil dilatancy; m can be determined from Equation (18) at the phase transformation state when $d = \frac{d\varepsilon_v^p}{d\varepsilon_q^p} = 0$, $\psi^* = {\psi^*}_{PTS}$, and $\eta = \eta_{PTS}$, thus

$$m = \frac{1}{{\psi^*}_{PTS}} \ln\left(\frac{\eta_{PTS}}{M_{cs}^*(W_{total})}\right). \tag{23}$$

The parameter d_0 can be calculated at the peak deviator point, i.e. $d = d_{peak}$, $\psi^* = {\psi^*}_{peak}$, and $\eta = \eta_{peak}$, hence,

$$d_0 = \frac{d_{peak}}{\left(e^{m{\psi^*}_{peak}} - \frac{\eta_{peak}}{M_{cs}^*(W_{total})}\right)}. \tag{24}$$

h_0 is the hardening parameter and it can be calculated by fitting the relationship between the volumetric strain ε_v and the shear strain ε_q.

Model Validation and discussion

This proposed constitutive model was validated by comparing the test data with the model predictions. Figs.7-9 compare the model predictions for static stress-strain curves with the available test data. It is evident that the bounding surface model based on the critical state framework accurately captures the overall stress-strain relationship and the volumetric response for SFS+CW+RC mixtures. In view of the behaviour shown in Figs.7-9, all the SFS+CW+RC mixtures with $R_b < 30\%$ present a strain-softening behaviour accompanied by a contractive-dilative response. As R_b increases, (a) the peak deviator stress decreases, (b) the stress-strain curve of the granular waste mixtures changes from brittle to ductile, (c) the strain softening changes to strain hardening, and (d) the specimen becomes more contractive. The effect of R_b on the stress-strain behaviour of sand-RC mixtures is similar to that for the SFS+CW+RC matrix as shown in Fig.10. As expected, when ${\sigma'}_3$ increases, both the peak deviator stress and strain hardening increase (Fig.11). Also, when ${\sigma'}_3$ increases, the compression is greater at lower axial strain (<10%) and dilation occurs subsequently, with the specimen at a lower σ'_3 dilating at a faster rate. Specifically, in Fig.11, compared to the model proposed by Youwai and Bergado (2003), the current model can capture the stress-strain behaviour of sand-RC mixtures even better, because the critical state parameters are more realistically determined by relating them to the work input and R_b (%) whereas the end-of-test state was assumed as the critical state by Youwai and Bergado (2003).

There is a noticeable deviation between the laboratory test results and predictions based on the constitutive model for the stress-stain curves when $\varepsilon_1 < 5\%$. This is attributed to the possible underestimation of elastic properties. In the bounding surface plasticity theory, the purely elastic region is regarded as insignificant. This is generally in agreement with experimental evidence for granular materials where purely elastic strain was observed in the order of 0.00001 (Bellotti et al. 1989). However this may not be the same for the rubber-soil mixtures as rubber materials are more elastic than conventional hard aggregates, hence the elastic strains are more when rubber is introduced. This can be considered as a limitation of the analysis. Moreover, even with extreme experimental care, ideal conditions (e.g. homogeneous mixing to obtain uniform density, perfect loading conditions of test specimens etc.) cannot be always met, leading to some disparity between measured and predicted results.

The proposed model certainly has several limitations. The proposed bounding surface model is limited to compressive loading condition as the bounding surface is only defined for $q > 0$. Also, the empirical relationship between M_{cs} and W_{total} is only suitable for selected granular materials having variable M_{cs} under fully drained triaxial conditions. Back calculations are needed to obtain the critical state parameters (α and M_0). Therefore for conditions for which these granular materials cannot achieve a critical state, this empirical relationship can be used to obtain M_{cs}. Moreover, the rubber material in the mixtures is only limited to rubber crumbs or granulated rubber. Larger rubber particles (e.g. rubber chips) may keep deforming continually leading to excessive volumetric strain (compression), hence, may not conform to the above mentioned the critical state.

Conclusions

The addition of rubber crumbs (RC) can significantly influence the geotechnical behaviour of waste granular mixtures (SFS+CW+RC), especially at or approaching their critical state. It was found that the critical state parameters in $e - \ln p'$ space have a linear relationship with R_b (%), defining a more refined critical state surface in the $\mathrm{e} - \ln p' - R_b$ space, incorporating the influence of RC on the critical state of the waste matrix. Based on the relationship between M_{cs} and W_{total}, an alternative critical state surface is generated in the $q_{cs} - p_{cs} - W_{total}$ space capturing the effect of energy absorbing capacity of the waste matrix. Moreover, the empirical relationships of the critical state parameters in relation to the total work input W_{total} established for SFS+CW+RC mixtures could also be applied to selected sand-RC mixtures and other granular materials (e.g. ballast and rockfill) taken from past studies which show variable M_{cs}. In this way, the relevant material parameters that often do not attain a critical state in the laboratory can now be obtained more realistically using these empirical relationships.

Within the critical state framework, a constitutive model was proposed in this paper to predict the stress-strain behaviour of this waste granular matrix under static triaxial loading. The elasto-plastic deformation was quantified based on bounding surface plasticity. The energy absorbing capacity of the matrix was innovatively captured through a new relationship between M_{cs} and W_{total}. The bounding surface model was validated by comparing the model predictions with the test results of SFS+CW+RC mixtures conducted by the authors (Qi et al. 2018a), as well as using the available past data for sand-RC mixtures (Youwai and Bergado 2003). Excellent agreement between the model predictions and the test results was obtained.

Appendix 1 The Derivation equations for unit normal loading vector

The components of the loading direction vectors $\boldsymbol{n_p}$ and $\boldsymbol{n_q}$ can be determined as follows:

$$\boldsymbol{n_p} = \frac{\partial F/\partial \bar{p}'}{\sqrt{(\partial F/\partial \bar{p}')^2+(\partial F/\partial \bar{q})^2}} = \frac{M_{cs}^{*}(W_{total})\left[N\,ln\frac{\overline{p'}}{\overline{p'_c}}\right]^{\frac{1}{N}}\left[1+\left(N\,ln\frac{\overline{p'}}{\overline{p'_c}}\right)^{-1}\right]}{\sqrt{\left\{M_{cs}^{*}(W_{total})\left[N\,ln\frac{\overline{p'}}{\overline{p'_c}}\right]^{\frac{1}{N}}\left[1+\left(N\,ln\frac{\overline{p'}}{\overline{p'_c}}\right)^{-1}\right]\right\}^2+1}}, \tag{25}$$

$$\boldsymbol{n_q} = \frac{\partial F/\partial \bar{q}}{\sqrt{(\partial F/\partial \bar{p}')^2+(\partial F/\partial \bar{q})^2}} = \frac{1}{\sqrt{\left\{M_{cs}^{*}(W_{total})\left[N\,ln\frac{\overline{p'}}{\overline{p'_c}}\right]^{\frac{1}{N}}\left[1+\left(N\,ln\frac{\overline{p'}}{\overline{p'_c}}\right)^{-1}\right]\right\}^2+1}}. \tag{26}$$

Appendix 2 The Derivation equations for plastic modulus

To determine the plastic modulus $\boldsymbol{H_b}$ on the bounding surface, the following derivation equations are used:

$$\frac{\partial F}{\partial \bar{p}'_c} = -\frac{M_{cs}^*(W_{total})p'\left[N\ln(\frac{\overline{p'}}{p'_C})\right]^{\frac{1}{N}}}{\bar{p}'_c N\ln(\frac{\overline{p'}}{p'_C})}, \tag{27}$$

$$\frac{\partial \bar{p}'_c}{\partial {\varepsilon_v}^p} = \frac{1+e}{\lambda^*(R_b)-\kappa}, \tag{28}$$

$$\frac{\boldsymbol{m_p}}{\|\partial F/\bar{\boldsymbol{\sigma}}'\|} = \frac{d/\sqrt{1+d^2}}{\sqrt{(\partial F/\partial \bar{p}')^2+(\partial F/\partial \bar{q})^2}} = \tag{29}$$

$$\frac{d_0\left(e^{m\psi^*(R_b)}-\frac{\eta}{M_{cs}^*(W_{total})}\right)}{\sqrt{1+\left[d_0\left(e^{m\psi^*(R_b)}-\frac{\eta}{M_{cs}^*(W_{total})}\right)\right]^2}}\frac{1}{\sqrt{\left\{M_{cs}^*(W_{total})\left[N\,ln\frac{\overline{p'}}{p'_c}\right]^{\frac{1}{N}}\left[1+\left(N\,ln\frac{\overline{p'}}{p'_c}\right)^{-1}\right]\right\}^2+1}}.$$

Appendix 3 The governing equations

Based on the theory of bounding surface plasticity (Dafalias 1986), the governing equations for the stress-strain relationship are illustrated as follows:

$$\begin{bmatrix} dp' \\ dq \end{bmatrix} = \left(\boldsymbol{D}^e - \frac{\boldsymbol{D}^e \boldsymbol{m} \boldsymbol{n}^T \boldsymbol{D}^e}{\boldsymbol{H} + \boldsymbol{n}^T \boldsymbol{D}^e \boldsymbol{m}} \right) \begin{bmatrix} d\varepsilon_v \\ d\varepsilon_q \end{bmatrix} \tag{30}$$

where $\boldsymbol{D}^e$ is the elastic compliance defined by:

$$\boldsymbol{D}^e = \begin{bmatrix} K & 0 \\ 0 & 3G \end{bmatrix}, \tag{31}$$

where K is the tangential bulk modulus, and G is the tangential shear modulus. They can be determined by:

$$K = \frac{(1 + e_0)p'}{\kappa} \tag{32}$$

$$G = \frac{3(1 - 2\nu)}{2(1 + \nu)} K \tag{33}$$

where ν is the Poisson's ratio.

Notations

CS, CSL	= critical state, and the critical state line, respectively;
CW	= coal wash;
$\boldsymbol{D}^e$	= the elastic compliance;
d	= dilatancy
d_0	= dilatancy parameter;
d_{peak}	= dilatancy at peak deviatoric stress state;
dp', dq	= the increment of the effective mean stress and deviator stress, respectively;
$d\varepsilon_v, d\varepsilon_v^p$	= total, elastic, and plastic volumetric strain increment, respectively;
$d\varepsilon_q, d{\varepsilon_q}^p$	= total, elastic, and plastic deviator strain increment, respectively;
dW_{total}	= the increment of total work input;
e, e_0, e_{cs}	= void ratio, and the void ratio at initial state and critical state, respectively;
$e_{\kappa 0}$	= the void ratio when $p' = 1$ for the swelling line;
G, K, $\mathbf{H}$	= the shear, bulk, and hardening moduli, respectively;
$\boldsymbol{H_b}, \boldsymbol{H_\delta}$	= the plastic modulus at $\overline{\sigma}'$ on the bounding surface and the arbitrary modulus at σ', respectively;
h_0	= a scaling parameter controlling the steepness of the response in the $\varepsilon_v - \varepsilon_q$ plane;
m	= dilatancy parameter;
$\boldsymbol{m}, \boldsymbol{n}$	=the unit normal loading direction vector and the plastic flow direction vector, respectively;
$\boldsymbol{m_p}, \boldsymbol{m_q}$	= components of plastic flow direction vectors;
$\boldsymbol{n_p}, \boldsymbol{n_q}$	= are components of loading direction vectors;
N	= is a material constant controlling the curvature of the bounding surface;
M_0	= is the critical stress ratio when $W_{total} = 1\ kPa$;
M_{cs}	= the critical state stress ratio;
PTS	= phase transformation state;
p', p'_{cs}	= the effective mean stress and the effective mean stress at critical state (kPa), respectively;
$\bar{p}'_c, p'_C$	= the intercepts of the bounding surface and loading surface with the $q = 0$ axis, respectively;
q	= the deviatoric stress (kPa);
R	= the ratio between p' at the intercept of the loading surface with the M_{cs} line and the image point p'_C;
R_b	= the RC content (%);
RC	= rubber crumbs;
SFS	= steel furnace slag;
W_{total}	= the total work input up to failure (kPa);
α	= materials constant related to the total work input W_{total} and critical stress ratio M_{cs};
σ'_1, σ'_3	= the effective axial stress and the effective confining pressure (kPa), respectively;
ε_v, ε_q	= the volumetric strain and the deviatoric strain, respectively;
η	= the stress ratio;
η_{PTS}, η_{peak}	= the stress ratio at phase transformation state, and peak deviator stress state, respectively;

κ = the gradient of the swelling line
Γ^* = void ratio at $p'_{cs} = 1\ kPa$;
Γ_1, Γ_2 = calibration parameters for Γ^*;
λ^* = the gradient of the critical state line in $e - \ln p'$ space;
λ_1, λ_2 = calibration parameters for λ^*;
ν = Poisson's ratio;
ψ, ψ^* = state parameter and modified state parameter, respectively;
${\psi^*}_{peak}, \psi^*_{PTS}$ = modified state parameter at peak deviatoric stress state and phase transformation state, respectively;
δ_{max}, δ = the distance from the stress origin and the current stress point to the image stress point, respectively.

Acknowledgements

The first author would like to acknowledge the financial assistance provided by the Australian Research Council Discovery Project (ARC-DP) and ARC Industry Transformation Training Centre for Advanced Rail Track Technologies (ITTC-Rail). The assistance provided by industry (ASMS, South 32, and Tyre Crumb Australia) in relation to the procurement of material used in this study is gratefully acknowledged. The assistance in the laboratory from Mr. Richard Berndt and the occasional technical feedback from A/Prof Cholachat Rujikiatkamjorn and Dr Trung Ngo are appreciated.

References

Ajmera, B., Tiwari, B., Koirala, J. and Obaid, Z. (2017). “Compaction characteristics, unconfined compressive strengths, and coefficients of permeability of fine-grained soils mixed with crumb-rubber tire.” *J. Mater. Civil Eng.*, 29(9), 04017148.

Been, K., and Jefferies, M.J. (1985). “A state parameter for sands.” *Géotechnique,* 35(2), 99-112.

Been, K., Jefferies, M.J. and Hachey, J. (1991). “The critical states of sands.” *Géotechnique,* 41(3), 365-381.

Bellotti, R., Ghionna, V., Jamiolkowski, M., Robertson, P.K. and Peterson R.W. 1989. “Interpretation of moduli from self-boring pressuremeter tests in sand”. *Géotechnique,* 39(2), 269-292.

Carrera, A., Coop, M. and Lancellotta, R. (2011). “Influence of grading on the mechanical behavior of Stava tailings”. *Géotechnique*, 61(11), 935-946.

Chavez, C. and Alonso, E.E. (2003). “A constitutive model for crushed granular aggregates which includes suction effects.” *Soil and Foundations,* 43(4), 215-227.

Chiaro, G., Indraratna, B. and Tasalloti, S.M.A. (2015), “Predicting the behaviour of coal wash and steel slag mixtures under triaxial conditional”. *Can. Geotech. J.,* 52, 1-7.

Chiaro, G., Indraratna, B., Tasalloti, S.M.A. and Rujikiatkamjorn, C. (2013), “Optimisation of coal wash-slag blend as a structural fill”. *Ground Improvement,* 168(GI1), 33-44.

Coop, M.R. (1990). “The Mechanics of Uncemented Carbonate Sands”. *Géotechnique* 40(4), 607-626.

Coop, M.R., Sorensen, K.K., Bodas Freitas, T. and Georgoutsos, G. (2004). “Particle breakage during shearing of a carbonate sand.” *Géotechnique,* 54(3), 157-163.

Dafalias, Y.F. (1986). “Bounding surface plasticity, I: Mathematical foundation and hypoplasticity.” *Journal of Engineering Mechanics, ASCE*, 112(9), 966-987.

Dafalias, Y.F. and Popov, E.P. (1975). “A model for nonlinearly hardening materials for complex loading.” *Acta Mechanica*, 21, 173-192.

Disfani, M.M., Tsang, H.H., Arulrajah, A. and Yaghoubi, E. (2017). “Shear and compression characteristics of recycled glass-tire mixtures.” *J. Mater. Civil Eng.*, 29(6), 06017003.

Fu, R., Coop, M.R. and Li, X.Q. (2014). “The mechanics of a compressive sand mixed with tyre rubber”. *Géotechnique Letters*, 4(3), 238-243.

Fu, R., Coop, M.R. and Li, X.Q. (2017). “Influence of particle type on the mechanics of sand-rubber mixtures”. *J. Geotech. Geoenviron. Eng.*, 143(9), 04017059.

Heitor, A., Indraratna, B., Kaliboullah, C., Rujikiatkamjorn, C. and McIntosh, G. (2016). “Drained and undrained shearing behavior of compacted coal wash.” *J. Geotech. Geoenviron. Eng.*, 142(5), 04016006.

Indraratna, B., Gasson, I. and Chowdhury, R. N. (1994). “Utilization of compacted coal tailings as a structural fill.” *Can. Geotech. J.*, 31(5), 614-623.

Indraratna, B., Sun, Q.D. and Nimbalkar, S. (2015). “Observed and predicted behaviour of rail ballast under monotonic loading capturing particle breakage.” *Can. Geotech. J.*, 52, 73-86.

Indraratna, B., Qi, Y. and Heitor, A. (2018). “Evaluating the Properties of Mixtures of Steel Furnace Slag, Coal Wash, and Rubber Crumbs Used as Subballast.” *J. Mater. Civil Eng.*, 30(1), 04017251.

Khalili, N., Habte, M.A. and Zargarbashi, S. (2008). “A fully coupled flow deformation model for cyclic analysis of unsaturated soils including hydraulic and mechanical hystereses.” *Computers and Geotechnics*, (35), 872-889.

Lackenby, J., Indraratna, B., Mcdowell, G. and Christie, D. (2007). “Effect of confining pressure on ballast degradation and deformation under cyclic triaxial loading”. *Géotechnique*, 57(6), 527-536.

Lee, J.H., Salgado, R., Bernal, A. and Lovell, C.W. (1999). "Shredded tires and rubber-sand as lightweight backfill." *J. Geotech. Geoenviron. Eng.*, 125(2), 132-141.

Li, B., Huang, M.S. and Zeng, X.W. (2016). "Dynamic behavior and liquefaction analysis of recycled-rubber sand mixtures." *J. Mater. Civil Eng.*, 28(11), 04016122.

Li, X.S. and Dafalias, Y.F. (2000). "Dilatancy for cohesionless soils." *Géotechnique*, 50(4), 449-460.

Lizarazo-Marriaga, J., Claisse, P. and Ganjian, E. (2011). "Effect of steel slag and portland cement in the rate of hydration and strength of blast furnace slag pastes." *J. Mater. Civil Eng.*, 23(2), 153-160.

Malasavage, N., Jagupilla, S., Grubb, D., Wazne, M. and Coon, W. (2012). "Geotechnical Performance of Dredged Material—Steel Slag Fines Blends: Laboratory and Field Evaluation." *J. Geotech. Geoenviron. Eng.*, 138(8), 981-991.

Mashiri, M., Vinod, J. and Sheikh, M. (2015a). "Constitutive model for sand–tire chip mixture." *International Journal of Geomechanics*, 16(1), 04015022.

Mashiri, M., Vinod, J.S., Sheikh, M.N. and Carraro, J.A.H. (2017). "Shear modulus of sand–tire chip mixtures". *Environmental Geotechnics*, 16.00016.

Mashiri, M., Vinod, J.S., Sheikh, M.N. and Tsang, H.H. (2015b). "Shear strength and dilatancy behaviour of sand–tire chip mixtures." *Soil and Foundations*, 55(3), 517-528.

Mohammadinia, A., Disfani, M.M., Narsilio, G.A. and Aye, L. (2018). "Mechanical behaviour and load bearing mechanism of high porosity permeable pavements utilizing recycled tire aggregates." *Construction and Building Materials*, 168, 794-804.

Qi, Y., Indraratna, B., Heitor, A. and Vinod, J.S. (2018b). "The Influence of Rubber Crumbs on the Energy Absorbing Property of Waste Mixtures." Proceedings of the International Symposium on Geotechnics of Transportation Infrastructure (ISGTI 2018). New Delhi, India.

Qi, Y., Indraratna, B., Heitor, A. and Vinod, J.S. (2018c). “Effect of Rubber Crumbs on the Cyclic Behaviour of Steel Furnace Slag and Coal Wash Mixtures.” *Journal of Geotechnical and Geoenvironmental Engineering*, 144(2), 04017107.

Qi, Y., Indraratna, B. and Vinod, J.S. (2018a). “Behavior of Steel Furnace Slag, Coal Wash, and Rubber Crumb Mixtures, with Special Relevance to Stress-dilatancy Relation.” *Journal of Materials in Civil Engineering*, 30(11), 04018276.

Russell, A.R. and Khalili, N. (2004). “A bounding surface plasticity model for sands exhibiting particles crushing.” *Can. Geotech. J*, 41, 1179-1192.

Russell, A.R. and Khalili, N. (2006). “A unified bounding surface plasticity model for unsaturated soils.” *International Journal for numberical and Analytical Methods in Geomechanics*, 30, 181-212.

Sheikh, M.N., Mashiri, M., Vinod, J. and Tsang, H. (2013). “Shear and compressibility behavior of sand-tire crumb mixtures.” *J. Mater. Civil Eng.*, 25(10), 1366-1374.

Shi, C. 2004. “Steel Slag-Its Production, Processing, Characteristics, and Cementitious Properties”, *J. Mater. Civ. Eng.*, 16, 230-236.

Sun, Y.F., Xiao, Y. and Wen, J. (2014). “Bounding surface model for ballast with additional attention on the evolution of particle size distribution.” *Science China Technological Sciences*, 57,1352-1360.

Tasalloti, S.M.A., Indraratna, B., Rujikiatkamjorn, C., Heitor, A. and Chiaro, G. (2015). “A laboratory Study on the Shear Behavior of Mixtures of Coal Wash and Steel Furnace Slag as Potential Structural Fill.” *Geotechnical testing journal*, 38(4), 361-372.

Tsang, H.H., Lo, S.H., Xu, X. and Sheikh, M.N. (2012). “Seismic isolation for low-to-medium-rise buildings using granulated rubber-soil mixtures: Numerical study.” *Earthquake Eng. Struct. Dyn.*, 41(14), 2009-2024.

Wang, G., Wang, Y. and Gao, Z. (2010). “Use of Steel Slag as a Granular Material: Volume Expansion Prediction and Usability Criteria.” *J. Hazard. Mater.*, 184, 555-560.

Wroth, M.A. and Bassett, B. (1965). “A stress-strain relationship for the shearing behaviour of a sand.” *Géotechnique*, 15(1), 32-56.

Xue, Y., Wu, S., Hou, H. and Zha, J. (2006). “Experimental investigation of basic oxygen furnace slag used as aggregate in asphalt mixture.” *J. Hazard. Mater.*, 138(2), 261-268.

Yaghoubi, M., Shukla, S.K. and Mohyeddin, A. (2018). “Effects of addition of waste tyre fibres and cement on the engineering behaviour of Perth sand.” *Geomechanics and Geoengineering*, 13(1), 42-53, DOI: 10.1080/17486025.2017.1325941.

Yildirim, I.Z. and Prezzi, M. (2015). “Geotechnical properties of fresh and aged basic oxygen furnace steel slag.” *J. Mater. Civ. Eng.*, 27(12), 04015046-1-11.

Youwai, S. and Bergado, D.T. (2003). “Strength and deformation characteristics of shredded rubber tire-sand mixtures.” *Can. Geotech. J.*, 40(2), 254-264.

Zornberg, J.G., Viratjandr, C. and Cabral, A.R. (2004). “Behaviour of tire shred–sand mixtures.” *Can. Geotech. J.*, 41(2), 227-241.

Figure list

Fig.1 (a-b) Critical state line (CSL) and phase transformation state (PTS) line in p’-q plane; (c-d) stress ratio-dilatancy curve of SFS+CW+RC mixtures

Fig.2 The relationship of W_{total} and critical stress ratio M_{cs} for: (a) SFS+CW+RC mixtures (data from Qi et al., 2018, (b) Sand-RC mixtures (data from Youwai and Bergado, 2003), (c) Ballast (data from Indraratna et al., 2015), and (d) Saturated and unsaturated rockfill (data sourced from Chavez and Alonso, 2003)

Fig.3 Critical state surface based on W_{total} for SFS+CW+RC mixtures

Fig.4 CSL in $e - \ln p'$ space and the critical state parameters

Fig.5 Critical state surface for SFS+CW+RC mixtures in $e - \ln p' - R_b$ space

Fig.6 Schematic representation of the bounding surface and loading surface in $q - p'$ plane

Fig.7 Test results and model prediction for waste mixtures with different RC contents under $\sigma'_3 = 10\ kPa$: (a) deviator stress-axial strain curves; (b) volumetric strain-axial strain curves

Fig.8 Test results and model prediction for waste mixtures with different RC contents under $\sigma'_3 = 40\ kPa$: (a) deviator stress-axial strain curves; (b) volumetric strain-axial strain curves

Fig.9 Test results and model prediction for waste mixtures with different RC contents under $\sigma'_3 = 70\ kPa$: (a) deviator stress-axial strain curves; (b) volumetric strain-axial strain curves

Fig.10 Test results and model prediction for Sand-RC mixtures with different RC contents under $\sigma'_3 = 50\ kPa$ (data sourced from Youwai and Bergado, 2003): (a) deviator stress-axial strain curves; (b) volumetric strain-axial strain curves

Fig.11 Test results and model prediction for Sand60+RC40 (data sourced from Youwai and Bergado, 2003): (a) deviator stress-axial strain curves; (b) volumetric strain-axial strain curves

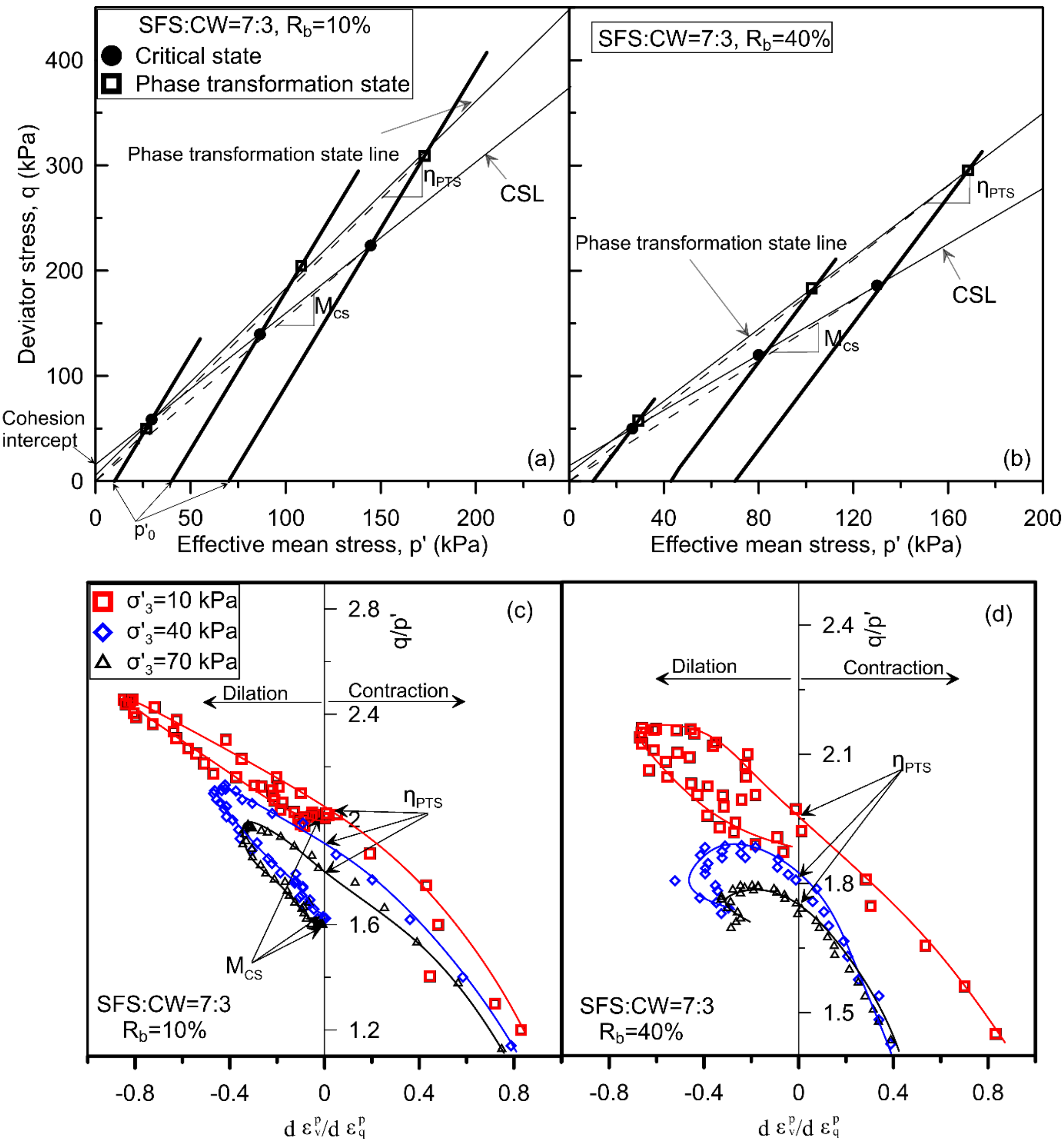

Fig.1 (a-b) Critical state line (CSL) and phase transformation state (PTS) line in p'-q plane; (c-d) stress ratio-dilatancy curve of SFS+CW+RC mixtures

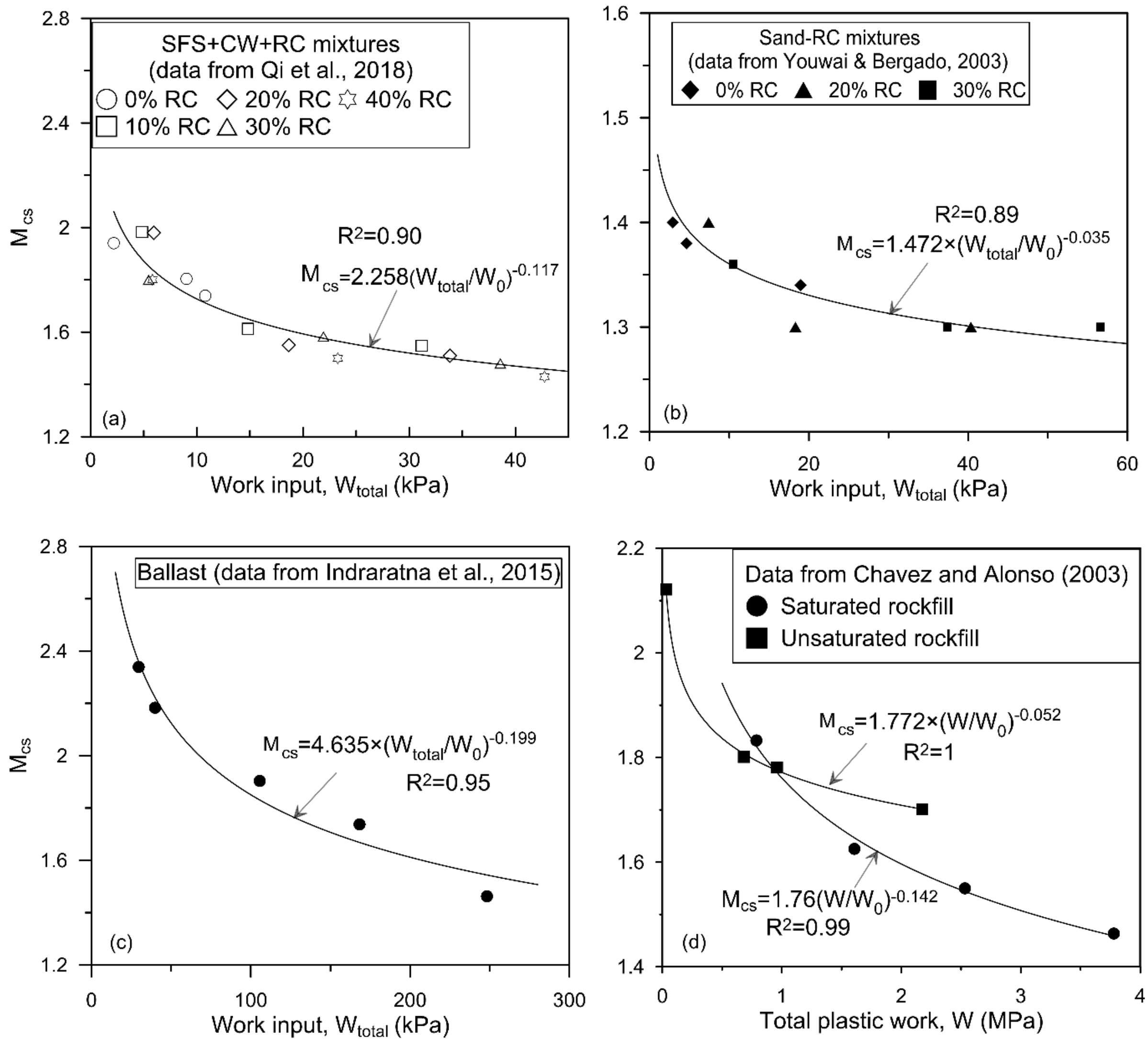

Fig.2 The relationship of W_{total} and critical stress ratio M_{cs} for: (a) SFS+CW+RC mixtures (data from Qi et al., 2018, (b) Sand-RC mixtures (data from Youwai and Bergado, 2003), (c) Ballast (data from Indraratna et al., 2015), and (d) Saturated and unsaturated rockfill (data sourced from Chavez and Alonso, 2003)

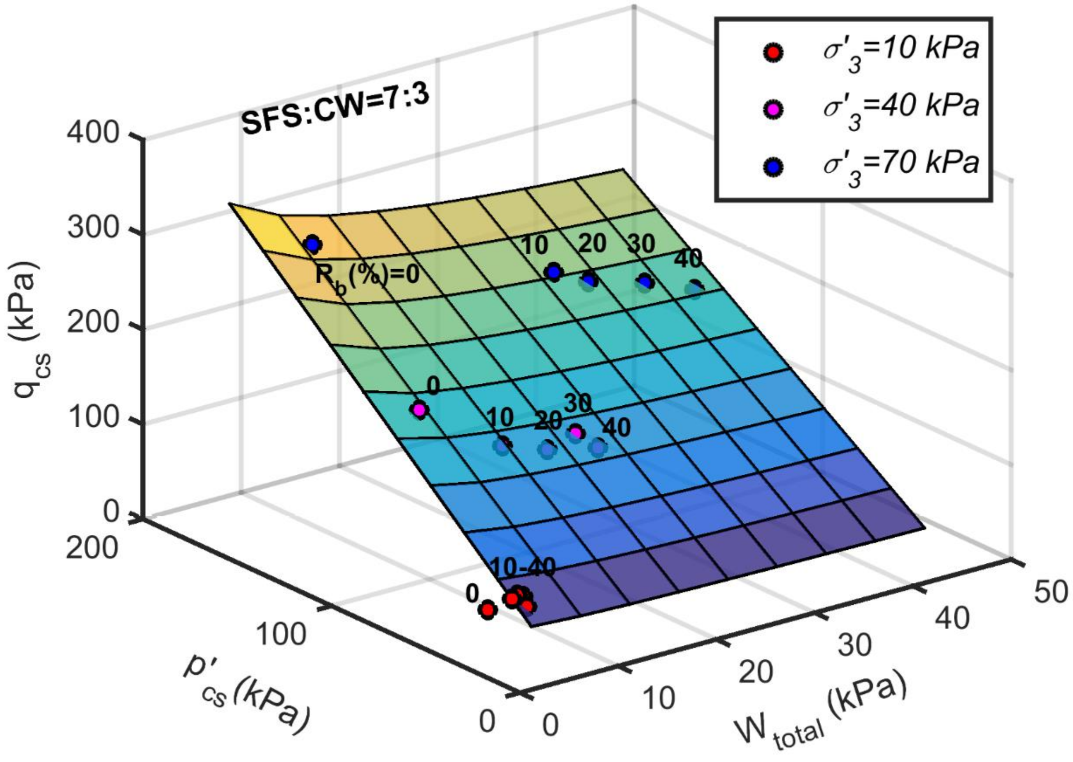

Fig.3 Critical state surface based on W_{total} for SFS+CW+RC mixtures

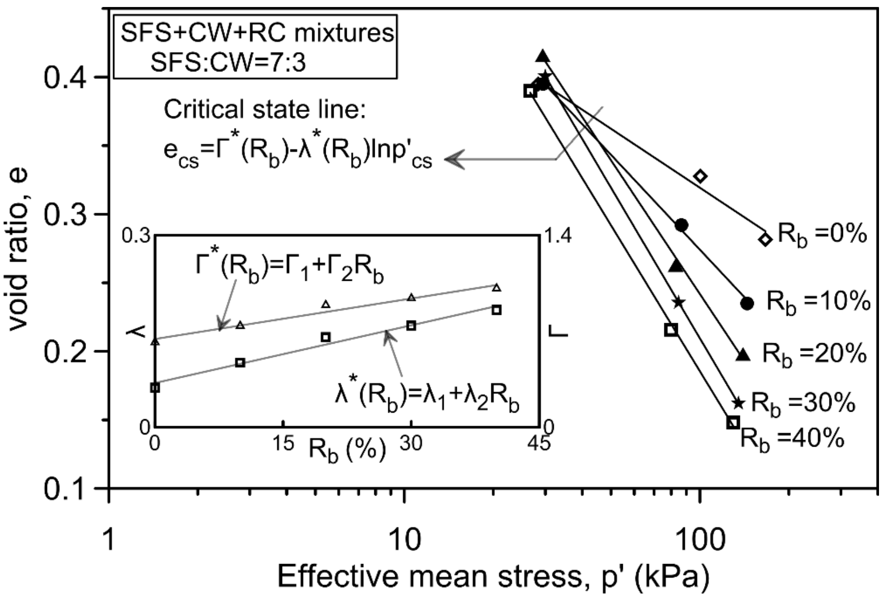

Fig.4 CSL in $e-\ln p'$ space and the critical state parameters

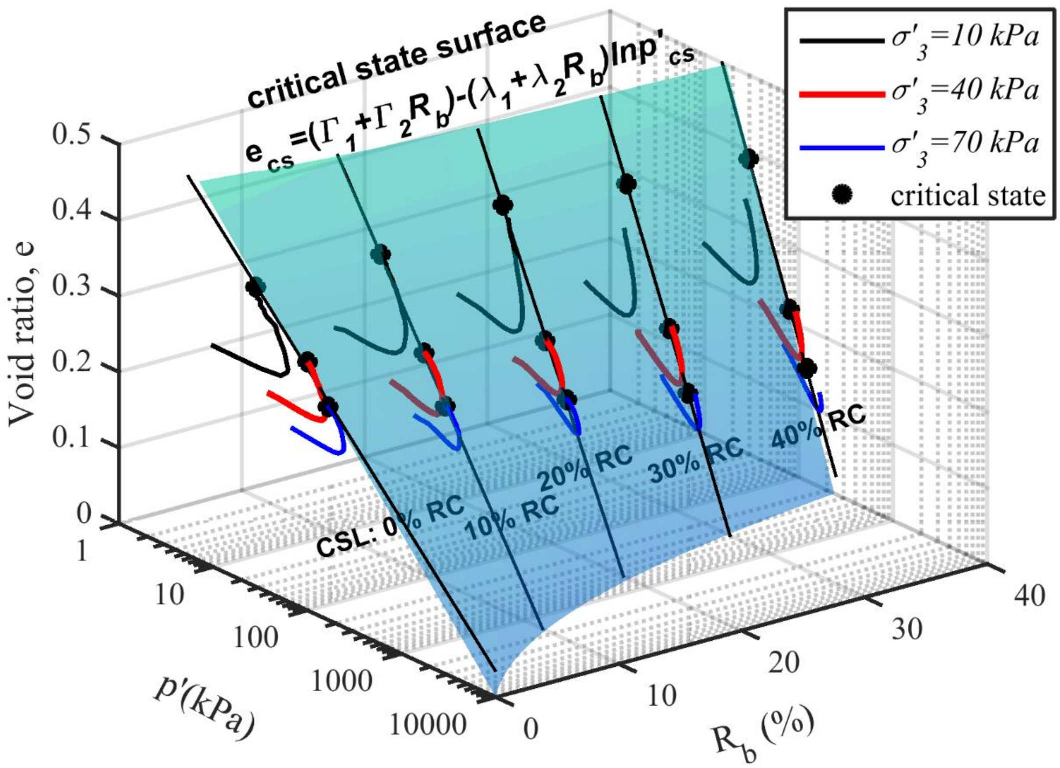

Fig.5 Critical state surface for SFS+CW+RC mixtures in $e - \ln p' - R_b$ space

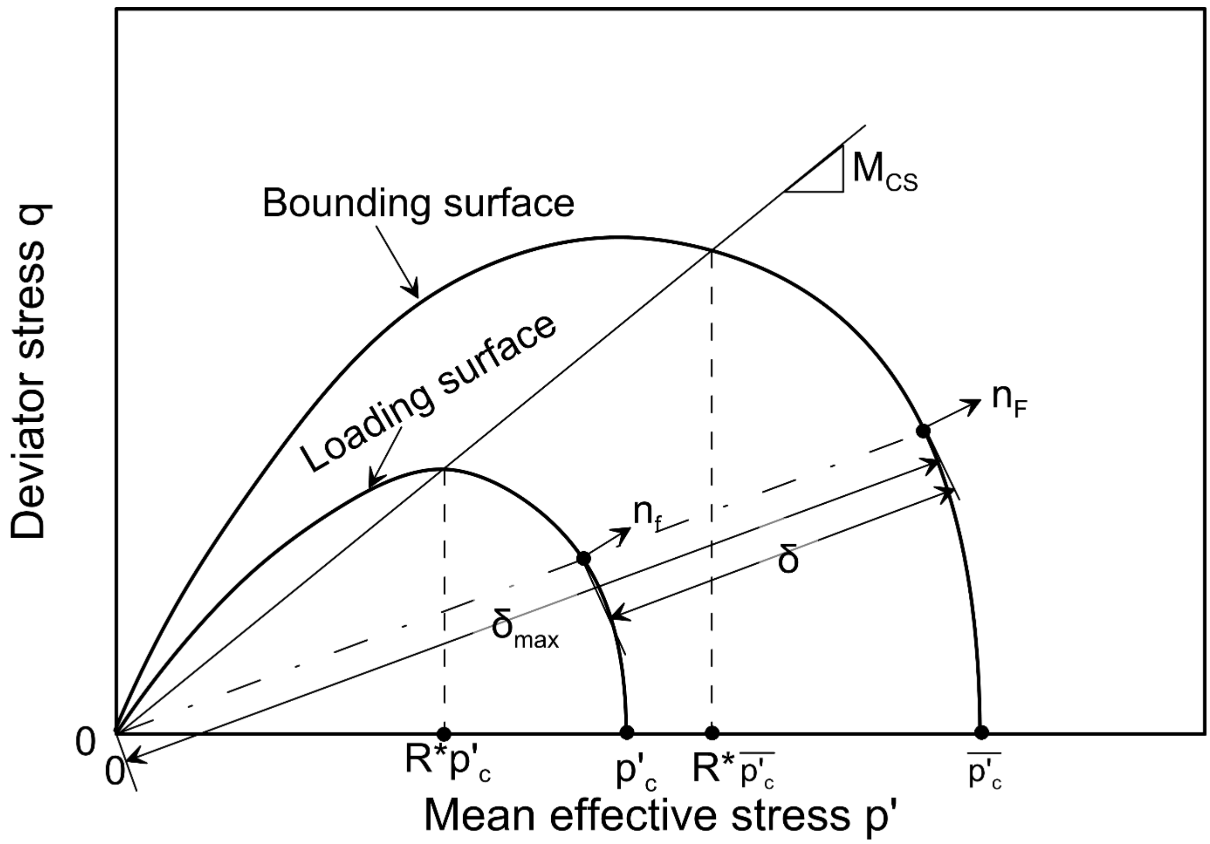

Fig.6 Schematic representation of the bounding surface and loading surface in $q - p'$ plane

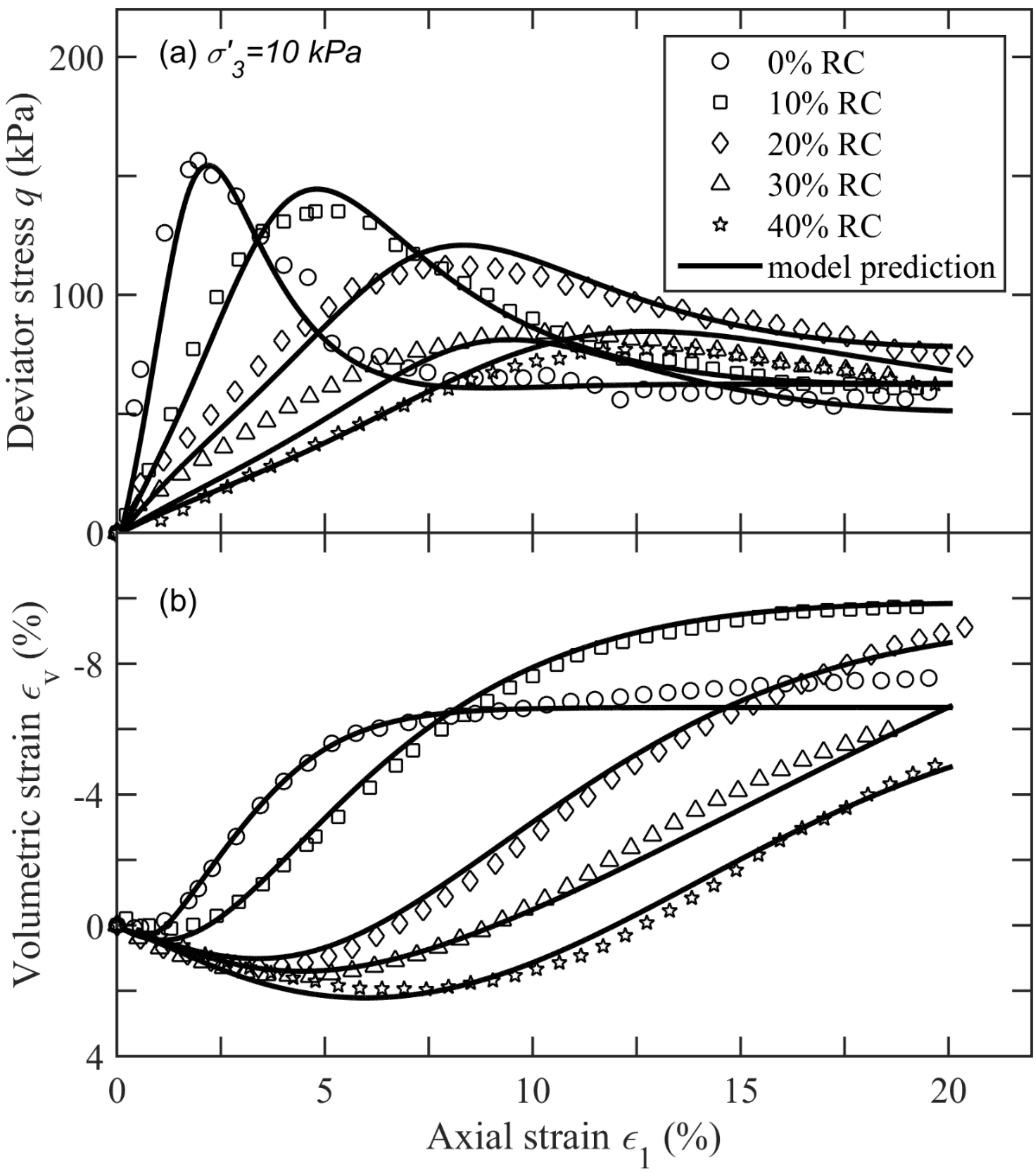

Fig.7 Test results and model prediction for waste mixtures with different RC contents under $\sigma'_3 = 10\ kPa$: (a) deviator stress-axial strain curves; (b) volumetric strain-axial strain curves

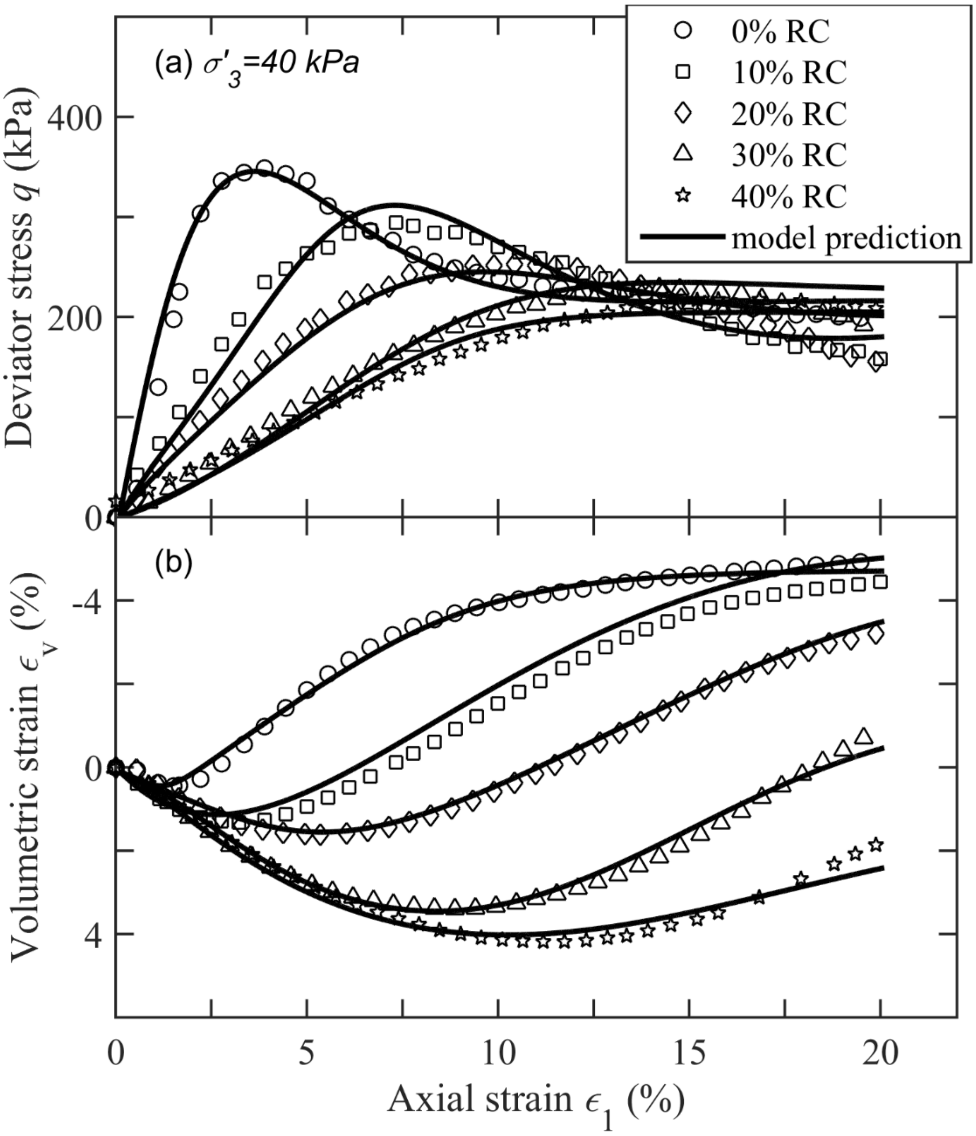

Fig.8 Test results and model prediction for waste mixtures with different RC contents under $\sigma'_3 = 40\ kPa$: (a) deviator stress-axial strain curves; (b) volumetric strain-axial strain curves

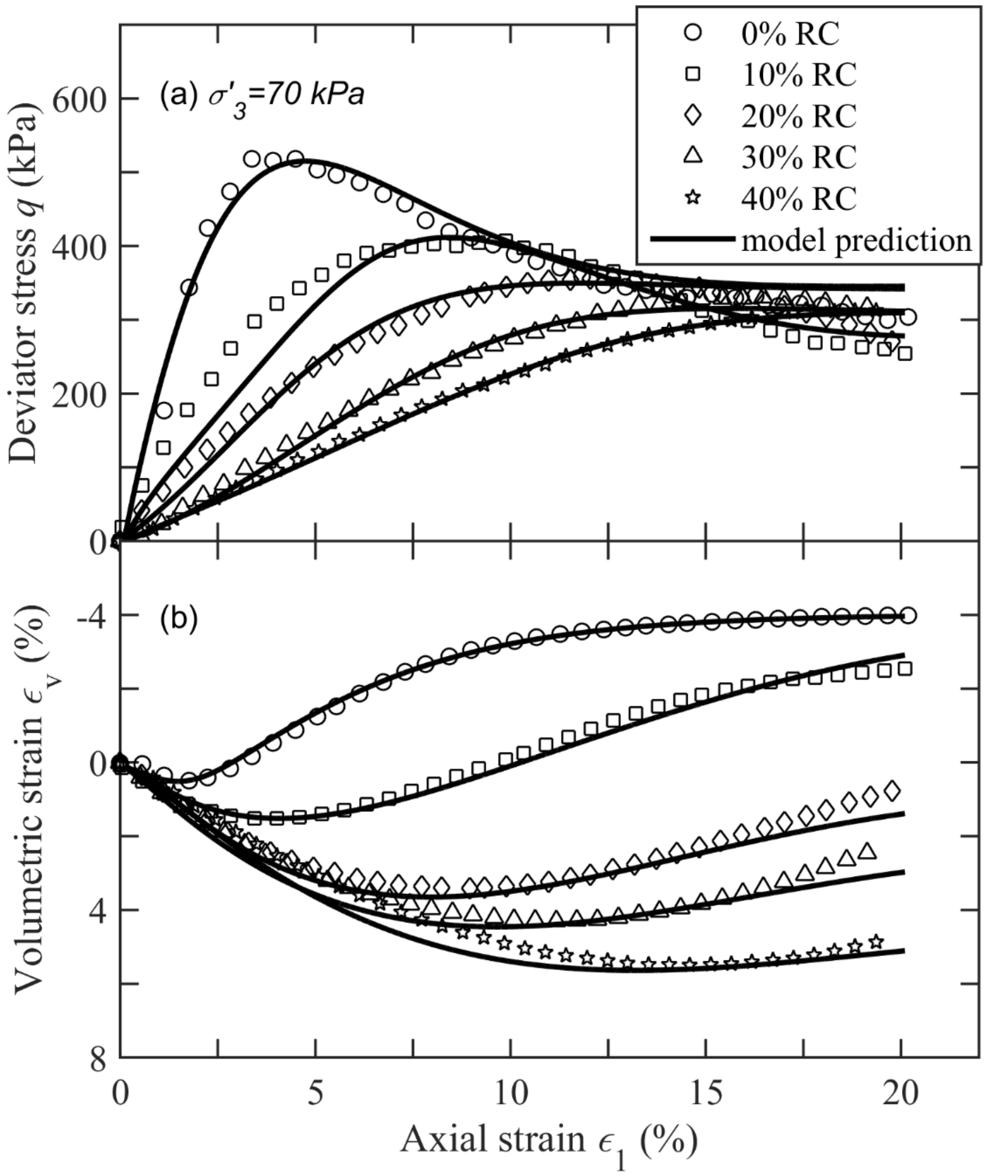

Fig.9 Test results and model prediction for waste mixtures with different RC contents under $\sigma'_3 = 70\ kPa$: (a) deviator stress-axial strain curves; (b) volumetric strain-axial strain curves

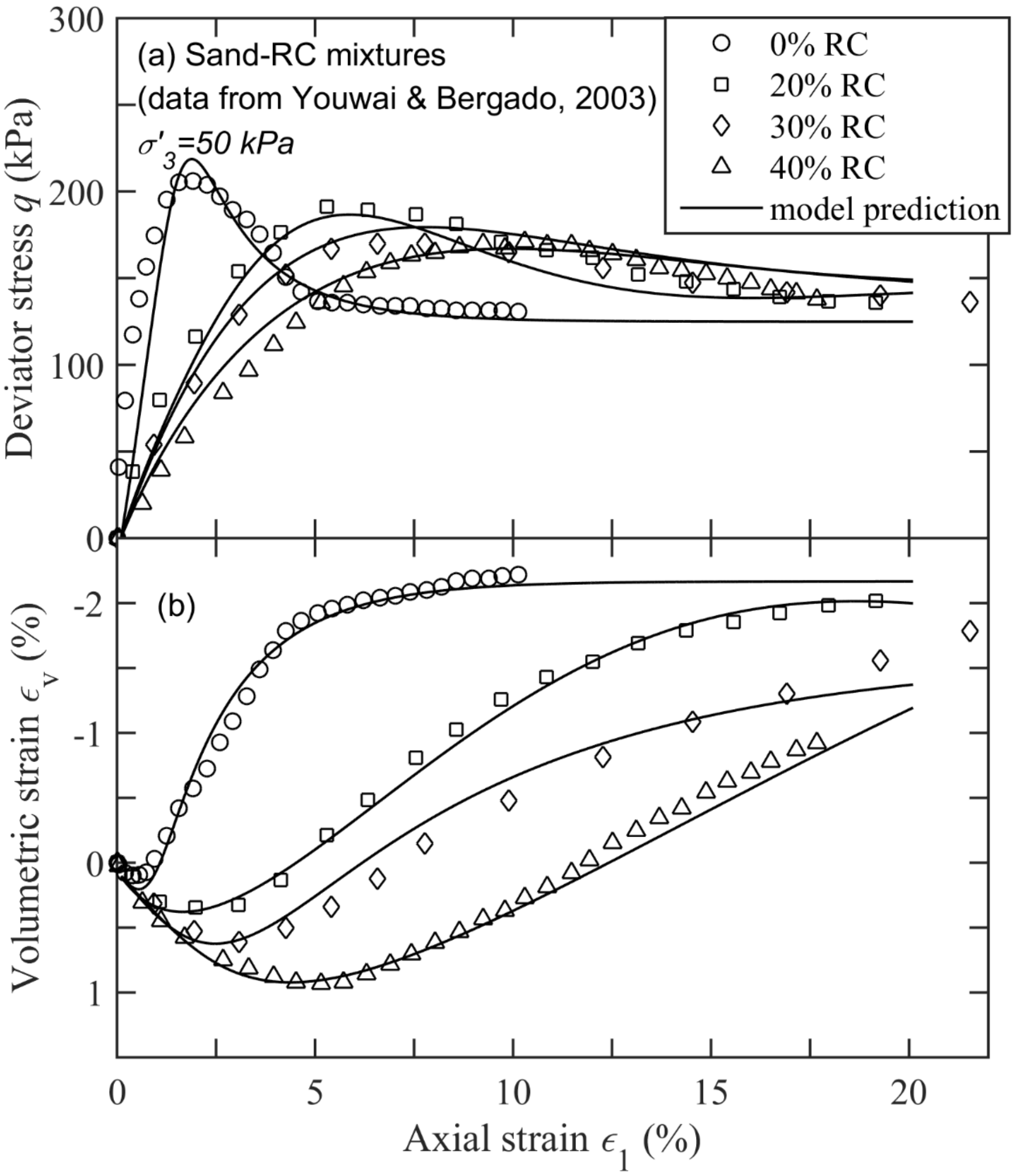

Fig.10 Test results and model prediction for Sand-RC mixtures with different RC contents under $\sigma'_3 = 50\ kPa$ (data sourced from Youwai and Bergado, 2003): (a) deviator stress-axial strain curves; (b) volumetric strain-axial strain curves

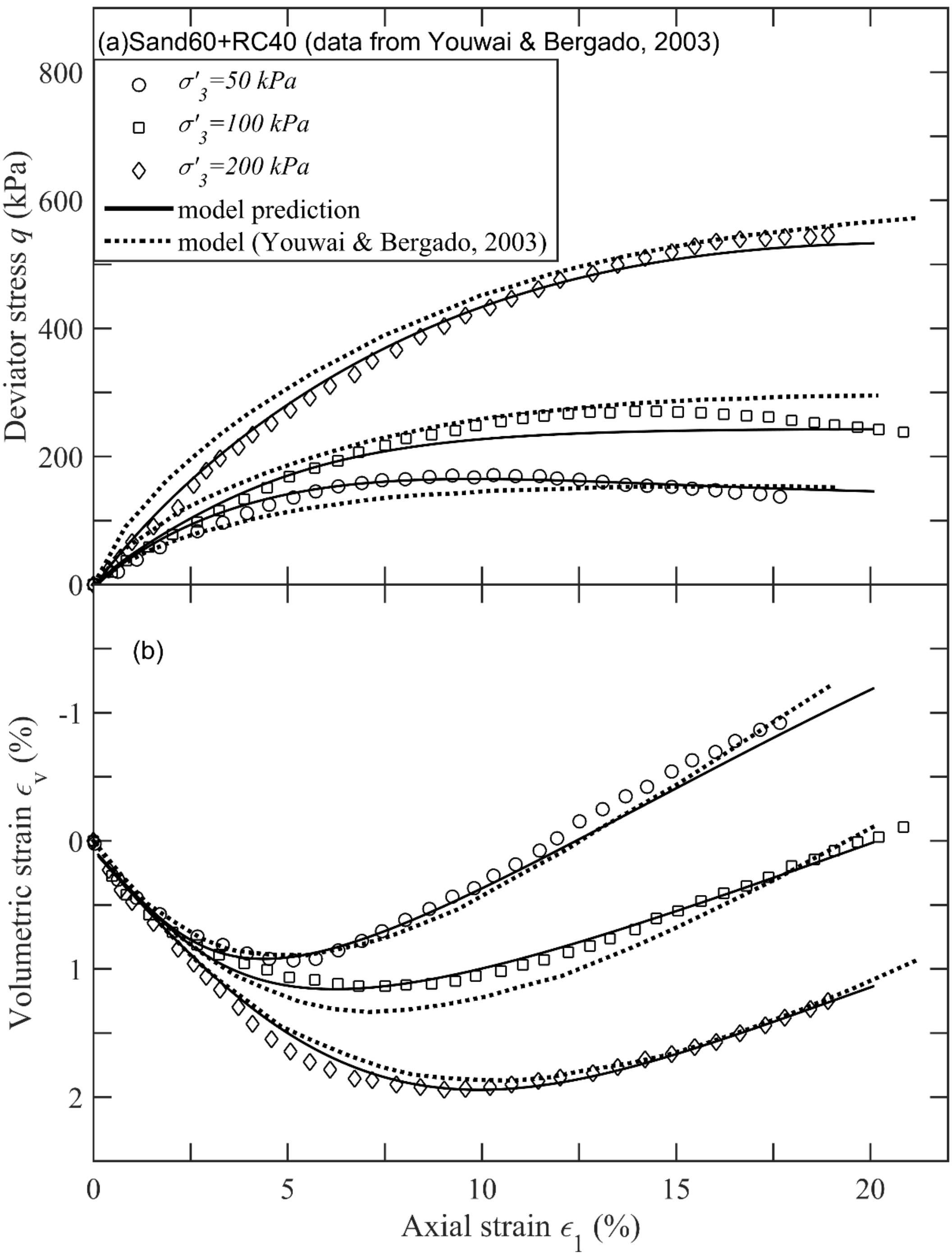

Fig.11 Test results and model prediction for Sand60+RC40 (data sourced from Youwai and Bergado, 2003): (a) deviator stress-axial strain curves; (b) volumetric strain-axial strain curves

Table list

Table 1 Parameters of critical state and dilatancy for current SFS+CW+RC mixtures and for previous Sand-RC mixtures

Data source	Mixtures	RC (%)	$\boldsymbol{\sigma'_3}$(kPa)	$\boldsymbol{m}$	$\boldsymbol{d_0}$	Critical state parameters
Qi et al., (2018a)	SFS70+CW30	0	10	-0.659	3.307	Γ_1 =0.64 $\Gamma_2 = 0.01$ $\lambda_1 = 0.069$ $\lambda_2 = 0.003$ $\mathrm{M}_0 = 2.258$ $\alpha = -0.117$
			40	-0.876	3.119	
			70	-1.30	3.03	
	SFS63+CW27+RC10	10	10	-0.46	2.95	
			40	-2.15	2.17	
			70	-2.86	1.83	
	SFS56+CW24+RC20	20	10	-0.53	5.12	
			40	-2.98	2.18	
			70	-5.29	3.19	
	SFS49+CW21+RC30	30	10	-0.93	3.80	
			40	-2.36	3.29	
			70	-4.16	2.49	
	SFS42+CW18+RC40	40	10	-0.556	6.014	
			40	-2.819	2.325	
			70	-4.307	2.890	
Youwai and Bergado, 2003	Sand100+RC0	0	50	0.2	1.045	$\Gamma_1 = 0.418$ Γ_2 =6.09$\times 10^{-3}$ λ_1 =-1.64$\times 10^{-3}$ λ_2 =1.04$\times 10^{-3}$ M_0 =1.472 $\alpha = -0.035$
			100	1.425	2.987	
			200	0.528	1.977	
	Sand80+RC20	20	50	-2.197	1.871	
			100	2.809	0.772	
			200	1.356	1.216	
	Sand70+RC30	30	50	-0.634	1.907	
			100	0.853	0.374	
			200	0.332	0.806	
	Sand60+RC40	40	50	-0.544	1.360	
			100	0.439	1.258	
			200	0.356	0.867	

Table 2 Hardening and elastic parameters for SFS+CW+RC mixtures and for previous studies

Data source	mixtures	R_b (%)	h_0	κ	υ
Data sourced from Qi et al., (2018a)			4.0	0.0020	0.29
	SFS63+CW27+RC10	10	2.5	0.0035	0.3
	SFS56+CW24+RC20	20	0.77	0.0048	0.31
	SFS49+CW21+RC30	30	0.88	0.0059	0.35
	SFS42+CW18+RC40	40	0.68	0.0063	0.35
Youwai and Bergado, 2003	Sand100+RC0	0	3.5	0.0046	0.33
	Sand80+RC20	20	0.8	0.0015	0.33
	Sand70+RC30	30	0.6	0.0053	0.33
	Sand60+RC40	40	0.5	0.0040	0.33